Available online at www.sciencedirect.com
ScienceDirect
Ceramics International 36 (2010) 1929–1935
CERAMICS INTERNATIONAL
www.elsevier.com/locate/ceramint

Clarifying the effect of sintering conditions on the microstructure and mechanical properties of β-tricalcium phosphate

Fidel H. Perera, Francisco J. Martínez-Vázquez, Pedro Miranda *, Angel L. Ortiz, Antonia Pajares

Departamento de Ingeniería Mecánica, Energética y de los Materiales, Universidad de Extremadura. Avda de Elvas s/n. 06071 Badajoz, Spain

Received 22 February 2010; received in revised form 3 March 2010; accepted 22 March 2010
Available online 21 May 2010

Abstract

The effect of the sintering conditions (temperature and time) on the microstructure (density and grain size) and mechanical properties (hardness, elastic modulus, and strength) of β-tricalcium phosphate (β-TCP) bioceramics fabricated from Ca-deficient commercial powders is analyzed. Contrary to current general opinion, it is demonstrated that the optimal sintering temperature to maximize the mechanical performance of this β-TCP material is not necessarily below the β ↔ α transformation temperature (1125 °C). In particular, optimal performance was achieved in samples sintered at 1200 °C for 3 h, since it was not until higher temperatures or longer sintering times that microcracking develops and mechanical properties are degraded. It is argued that the residual stresses developed during this reversible transformation do not lead to microcrack propagation until sufficiently large starting flaws develop in the microstructure as a consequence of grain growth. Implications of these findings for the processing routes to improve sintering of this important bioceramic are discussed.

Keywords: A. Sintering; C. Mechanical properties; Tricalcium phosphate; β-TCP

1. Introduction

Calcium phosphate materials are widely used in biomedical applications due to their osteoconductive and osteoinductive properties. In this context, hydroxyapatite (HA, $Ca_5[OH(PO_4)_3]$), the main mineral phase of bone, is an obvious first choice for orthopaedic implants. Nevertheless, its low biodegradability is a major handicap for those tissue engineering applications where the implanted material is intended to be resorbed and replaced by living tissue. Tricalcium phosphate (TCP, $Ca_3(PO_4)_2$), on the contrary, is progressively resorbed *in vivo* by a cell-mediated process and replaced by new bone [1–3], and is thus a more suitable candidate for this particular type of application. As shown in the phase diagram of Fig. 1, TCP can crystallize in three allotropic forms: β-TCP, which is stable from room-temperature up to 1125 °C, α-TCP, which is stable from 1125 °C up to 1470 °C, and α′-TCP which is stable from 1470 °C up to the melting point at 1810 °C [4]. Of the three variants, β-TCP is the most desirable in terms of chemical stability and bioresorption rate – α-TCP hydrolyses partially or completely into hydroxyapatite in a biological environment losing its resorbability [5], and α′-TCP cannot be stabilized at room temperature [4].

β-TCP is routinely used as bone replacement, especially in the field of oral and craniofacial surgery, in the form of granules and rods [5,6] or as filler in polymeric scaffolds [7]. In bulk, β-TCP bioceramics have mechanical properties too poor to be used in load-bearing clinical applications [8–10], which has been attributed to the difficulties in fully densifying β-TCP powders [9,11–13]. These difficulties are associated with the presumption that the sintering temperature should be kept below 1125 °C to avoid the β ↔ α phase transformation that is considered deleterious to mechanical properties. This is attributed to spontaneous massive microcracking in the sintered body due to the expansion-contraction cycle generated by the differences in density between β-TCP (3.07 g/cm^3) and α-TCP (2.86 g/cm^3) [10,11,14]. While this is accepted as a fact within the bioceramic community, to the best of the authors' knowledge no unambiguous proof that microcracking inherently follows the β ↔ α transformation exists in the literature.

* Corresponding author. Tel.: +34 924 28 96 00x86735; fax: +34 924 28 96 01.
E-mail address: pmiranda@unex.es (P. Miranda).

0272-8842/$36.00
doi:10.1016/j.ceramint.2010.03.015

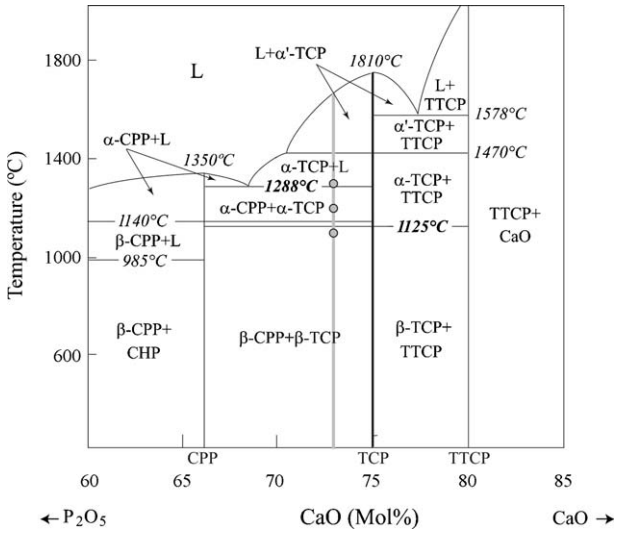

Fig. 1. Partial CaO–P_2O_5 equilibrium phase diagram [19]. The following notation is adopted to identify the phase composition: CHP: heptacalcium phosphate ($Ca_7(P_5O_{16})_2$), CPP: calcium pyrophosphate ($Ca_2O_7P_2$), TCP: tricalcium phosphate ($Ca_3(PO_4)_2$), and TTCP: tetracalcium phosphate ($Ca_4(PO_4)_2O$). The gray vertical line marks the composition of the starting powders and the circles indicate the sintering temperatures analyzed in this work.

With this in mind, the present study was conducted with the objective of investigating in more detail the effect of the sintering conditions on the microstructure and mechanical properties of β-TCP bioceramics, to clarify the role of the β ↔ α transformation on their mechanical degradation. The results challenge the accepted notion that sintering of these materials has to be carried out below the transformation temperature in order to obtain a good mechanical response. Based on these results, processing guidelines for fabricating β-TCP bioceramics with superior mechanical properties are proposed.

2. Experimental procedure

The β-TCP starting powder used in this study was obtained from a commercial source (Fluka, Buchs, Switzerland). This β-TCP powder is Ca-deficient (Ca/P molar ratio of 1.37 ± 0.03), and consists of micrometer particles with an average size of 1.8 ± 0.8 μm. The CaO molar concentration corresponding to this particular Ca/P ratio is marked in the phase diagram of Fig. 1 as a vertical light-gray line. The choice of a Ca-deficient (Ca/P < 1.5) powder is because the slow kinetics of the reverse α → β transformation in Ca-rich powders does not ensure the reversibility of the β ↔ α transformation [4,9]. Compacts were made by uniaxial pressing (C, Carver, Inc., Wabash, IN, USA) at 32 MPa, followed by isostatic pressing (CP360, AIP, Columbus, OH, USA) at 180 MPa. Pressureless sintering was performed in a conventional furnace (C.H.E.S.A, Madrid, Spain) under the following conditions: temperatures of 1100, 1200, and 1300 °C, times of 1, 3, 5, and 7 h, air atmosphere and heating and cooling rates of 10 °C/min. The sintering temperatures are indicated as circles on the composition line of Fig. 1. Surfaces for microstructural and mechanical characterizations were diamond-polished to 1 μm finish.

The starting powders and sintered samples were characterized by X-ray diffractometry (XRD, PW-1800, Phillips Research, The Netherlands) using Cu-Kα radiation and their phase composition was determined by the Rietveld method. Bulk samples were imaged using scanning electron microscopy (SEM, S-3600N, Hitachi, Japan) to analyze their microstructural evolution. Grain sizes were determined by routine image analysis (AnalySIS®, Olympus Soft Imaging Solutions GmbH, Germany) using random images totaling a minimum of 500 grains. In addition, the density, ρ, of the sintered samples was measured using the Archimedes method.

Berkovich indentation tests were performed on polished surfaces to evaluate the hardness and Young's modulus using a depth-sensing indentation instrument (NanoTest, Micro Materials, Wrexham, UK). For each sintering condition a total of 20 tests were conducted under ambient conditions at 10 N, with indentation load rate of 400 mN/s and dwell time of 10 s. Hardness and Young's modulus were evaluated from the indentation load-displacement curves using the Oliver and Pharr method [15]. The indentation sites were examined under optical microscopy (Nikon Epiphot 300, Nikon Corp., Japan) with Nomarski contrast.

For selected sintering conditions, larger specimens were prepared and cut into polished bars (25 mm × 5 mm × 5 mm) with chamfered edges to analyze their fracture behaviour. Flexural strength was determined using a four-point bending device – with outer and inner spans of 20 mm and 10 mm, respectively – assembled onto a universal testing machine (Instron Corp, Canton, MA). Tests were carried out at ambient conditions, using a crosshead speed of 15 mm/min.

3. Results and discussion

Fig. 2 shows SEM micrographs of the samples sintered at 1100, 1200, and 1300 °C for 1 and 7 h. These images evidence a significant grain growth produced with increasing sintering temperature and time. Microcracking is also evident in the samples sintered at 1300 °C (marked with arrows in Fig. 2e and f), but not in the rest. Nevertheless, extensive SEM observations revealed the presence of a few isolated microcracks in the samples sintered at 1200 °C for 5 and 7 h. The absence of microcracking at 1200 °C for 1 h and 3 h is an unexpected result because this temperature is above the β ↔ α transformation temperature of 1125 °C.

Apart from the microcracks, the SEM observations also show that the microstructure of the samples sintered at 1300 °C presents isolated regions with much finer grains (Fig. 2e and f). As shown in Fig. 3, the compositional maps obtained by EDS reveal that these regions are deficient in Ca with respect to the β-TCP matrix. No evidence for such a new microconstituent was observed in any case at 1100 and 1200 °C. Taken together, the morphology, chemical composition, and temperature at which the new microconstituent appears suggest that it originates from the recrystallization of a liquid phase. According to the phase diagram of Fig. 1, that new

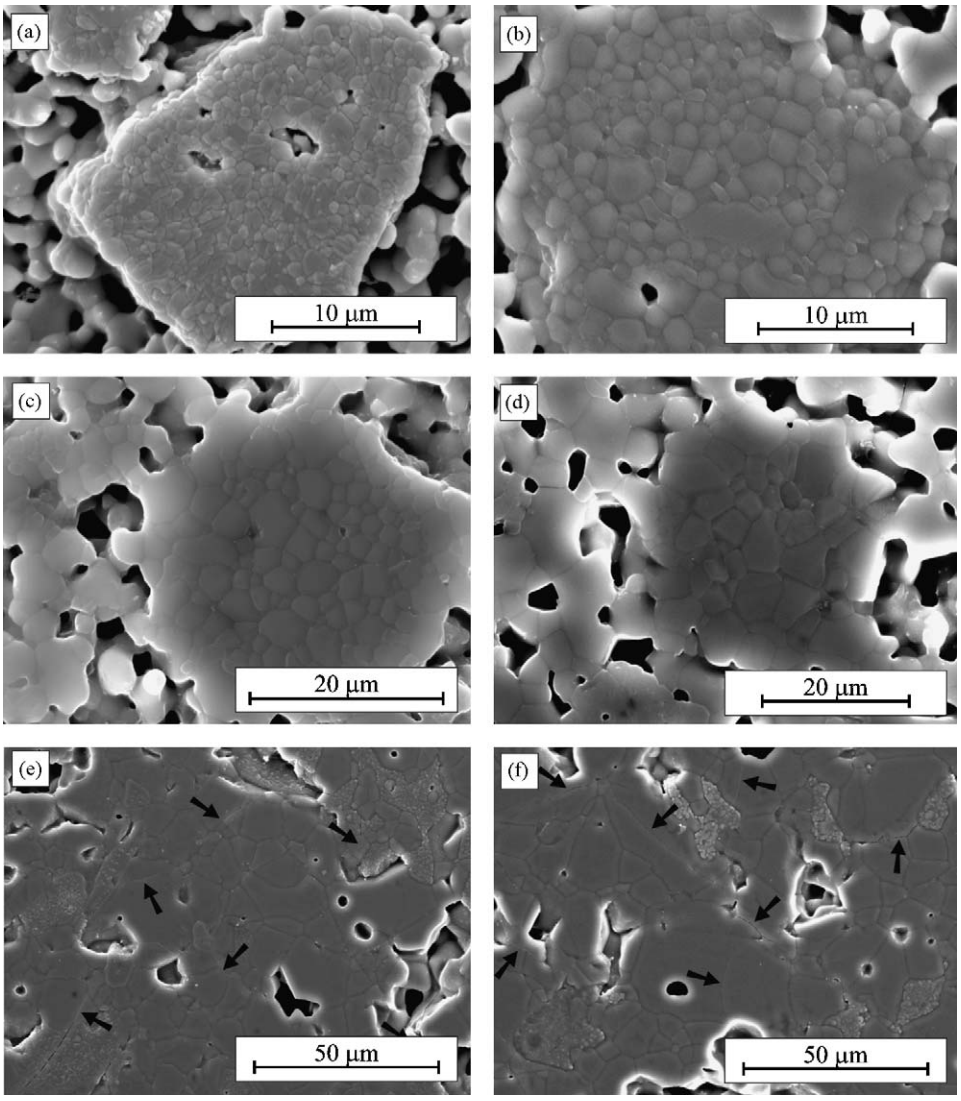

Fig. 2. SEM micrographs showing the microstructures of samples sintered for 1 h (left) and 7 h (right) at 1100 °C (a and b), 1200 °C (c and d), and 1300 °C (e and f). Differences in grain size and porosity are apparent (note scales). Arrows in (e and f) mark the presence of microcracks.

microconstituent would indeed result from the eutectic transformation of the liquid that forms above 1288 °C.

Fig. 4 compares the XRD patterns of the starting powders and of the samples sintered at 1200 °C for 7 h and at 1300 °C for 1 h. The comparison reveals that the phase composition of the starting powders is maintained up to 1300 °C. At this temperature, however, a new phase appears, identified as α-calcium pyrophosphate (*i.e.*, α-$Ca_2P_2O_7$, denoted α-CPP in the phase diagram of Fig. 1). The relative proportions of β-TCP and α-CPP determined by the Rietveld method are 84 ± 1 and 16 ± 1 wt.%, respectively. In addition, the phase composition of the samples sintered at 1300 °C is the same within the experimental error, regardless of the sintering time (1–7 h). Logically, the α-CPP grains are located in the Ca-deficient regions in Fig. 3.

The average grain size is plotted in Fig. 5 as a function of sintering time for each sintering temperature. The symbols represent experimental data, with standard deviation as error bars, and the lines are empirical fits. It has to be noted that the data corresponding to 1300 °C were calculated neglecting the small grains within the eutectic microconstituent since they originate from the recrystallization of a liquid phase during cooling, and therefore are not affected by sintering time. As can be seen, increasing sintering temperature and time produces significant grain growth in this material. Clearly, the effect of sintering temperature is more marked because diffusion is a thermally activated process.

As a consequence of the great susceptibility of this material to grain growth, its densification is very slow, as clearly evidenced in Fig. 6, which shows the density data as a function of time for the three sintering temperatures studied. Again, the symbols represent experimental data, with standard deviation as error bars, and the lines are linear fits to the data. The density increases with increasing sintering temperature but never reaches the theoretical value for β-TCP (3.07 g/cm^3). The densification rate is virtually zero (0.004 ± 0.003 g/cm^3 h) at 1100 °C, increases slightly at 1200 °C (0.035 ± 0.006 g/cm^3 h, around 1% increase in density per hour) and is slightly negative

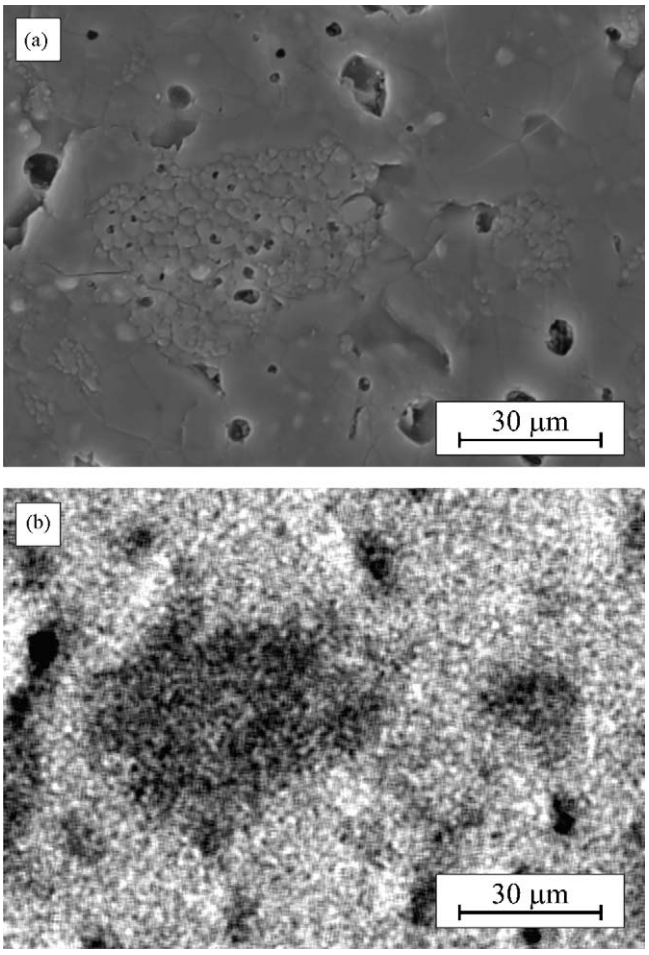

Fig. 3. SEM image (a) and Ca content mapping by EDS (b) of a β-TCP sample sintered at 1300 °C for 3 h. A new microconstituent, Ca-deficient compared to the matrix, is apparent (dark regions).

at 1300 °C (statistically significant as confirmed by one-way ANOVA test). This latter result is attributed to the increase in the number and size of cracks that have developed in the material, together with a negligible diffusion-induced densification rate with increasing sintering time, at this temperature. In any case, it is evident that a significant increase in density is achieved by increasing sintering temperature, especially up to 1300 °C because the presence of the liquid phase helps to fill the pores, significantly enhancing densification [9].

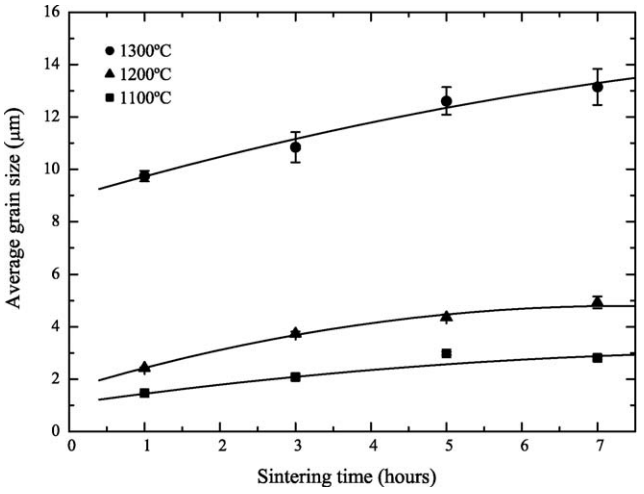

Fig. 5. Average grain size as a function of sintering time, for the indicated sintering temperatures. The symbols represent experimental data, with standard deviation as error bars, and the lines are empirical best-fits.

The improved densification translates into an increase in the hardness of the material with sintering temperature and time, as shown in Fig. 7a. However, elastic modulus data ($E^* = E/(1-\nu^2)$) obtained during the same Berkovich instrumented indentation tests, which are plotted in Fig. 7b, do not show the same trend. They first increase steadily up to 1200 °C at 3 h treatment and then drop to a nearly constant value. These results are explained by an increasing level of chipping around the imprint for sintering conditions above 1200 °C for 3 h. Indeed, since the elastic modulus in instrumented indentation is calculated from unloading data in the load *vs* penetration depth curve, if cracks appear in the material during loading the

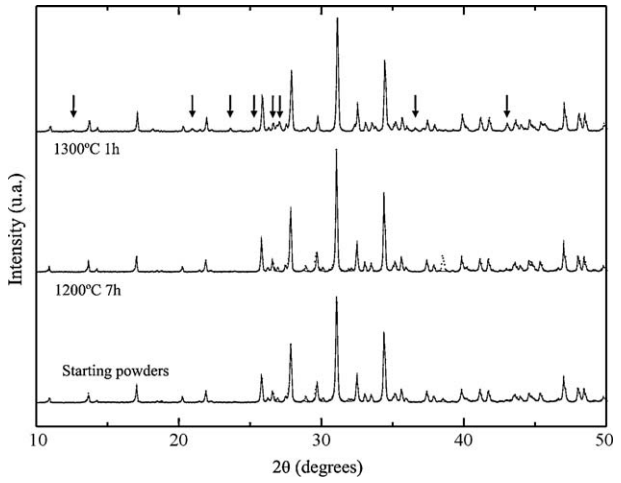

Fig. 4. XRD patterns corresponding to β-TCP starting powders and samples sintered at the indicated conditions. No phase transformation is observed up to 1300 °C where new peaks (arrows), corresponding to α-CPP, appear.

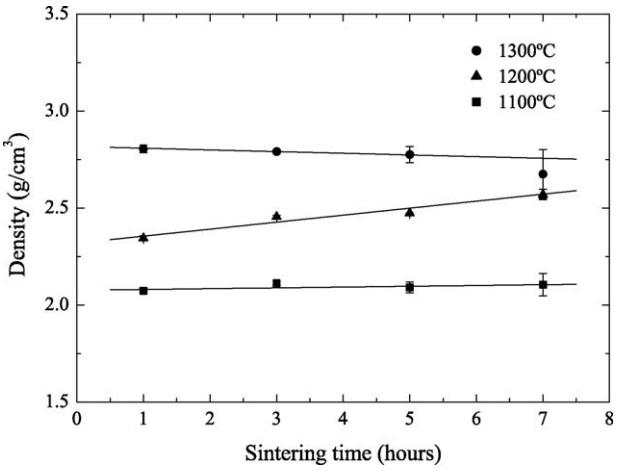

Fig. 6. Evolution of density with sintering time at the indicated temperatures. Symbols represent experimental data, with standard deviation as error bars, and lines are linear fits to data.

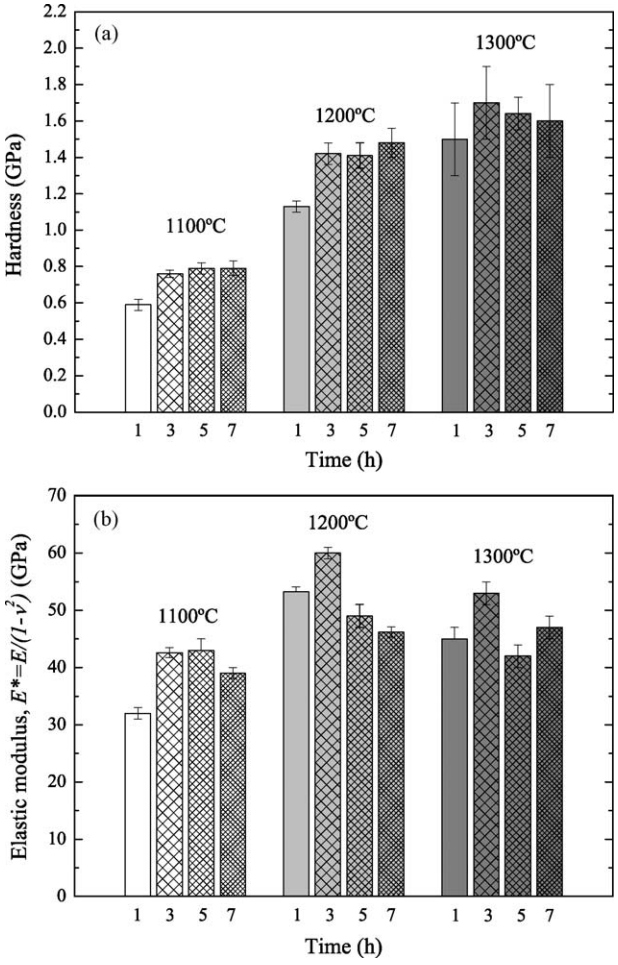

Fig. 7. Evolution of (a) hardness and (b) elastic modulus, $E^* = E/(1 - \nu^2)$, of β-TCP with temperature and sintering time. Average values from Berkovich instrumented indentation tests, with standard deviations as error bars.

measured values are lower than those expected for an undamaged material.

The optical images in Fig. 8 illustrate the aforementioned increase in chipping with sintering temperature by showing representative indentations on samples sintered for 3 h at the three selected temperatures. While chipping is not observable at 1100 °C (Fig. 8a) and hardly noticeable at 1200 °C (Fig. 8b), it is extensive at 1300 °C (Fig. 8c). Further evidence of the occurrence of chipping during indentations was the observation of an increasing number of pop-in events in the load-displacement curves as the sintering temperature and time increased. This increased level of chipping is attributed to the development of transformation-induced microcracking during sintering, which hints at a significant reduction in the strength of the material.

The reduction of strength hypothesized in the preceding paragraph is clearly evidenced in the results of Fig. 9. This figure shows the Weibull plot for the strength data obtained in 4-point bending tests performed on samples sintered for 3 h at the three selected temperatures. Samples sintered for 3 h were selected for these tests because they exhibited the best indentation results at each temperature. This plot shows the failure probability, P, as a function of applied stress, σ. The

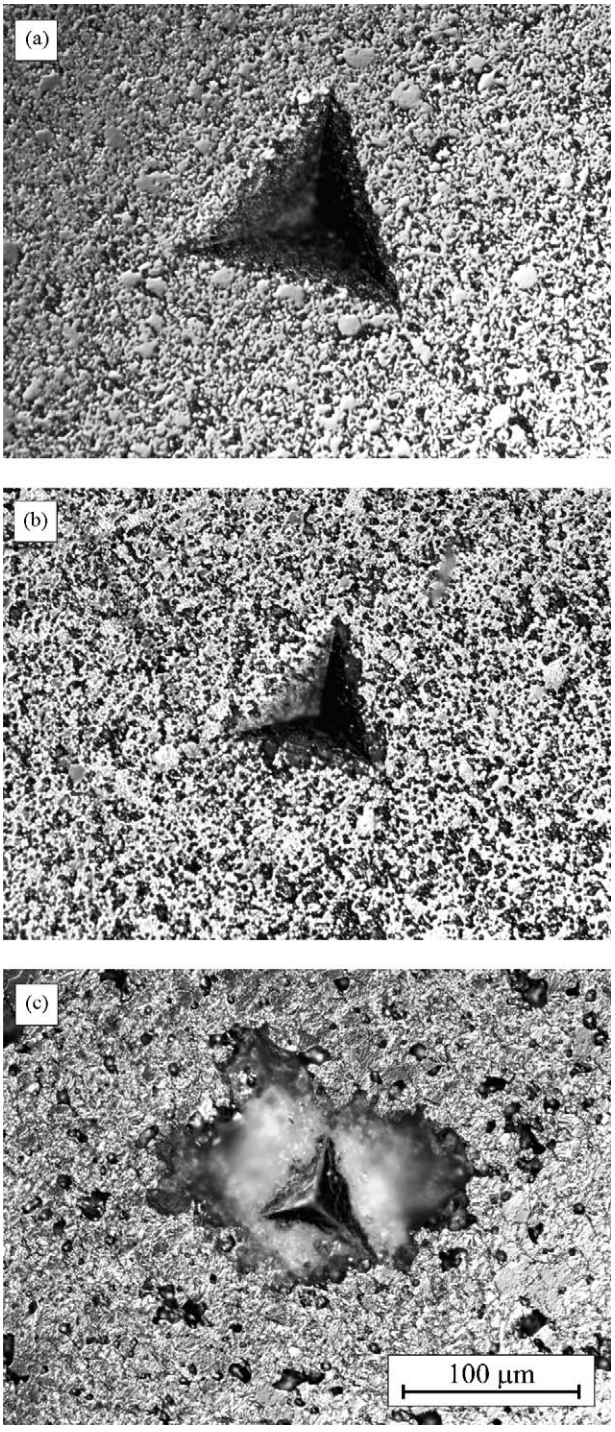

Fig. 8. Optical images with Nomarsky contrast showing representative indentation imprints on samples sintered for 3 h at (a) 1100 °C, (b) 1200 °C, and (c) 1300 °C and gold-coated after the tests. Extensive chipping is evident at 1300 °C.

straight lines are the best fits to data of the Weibull probability function [16–18],

$$P = 1 - \exp\left[-\left(\frac{\sigma}{\sigma_f}\right)^m\right] \quad (1)$$

where the Weibull modulus, m, and central value, σ_f, are adjustable parameters. This plot clearly shows that increasing

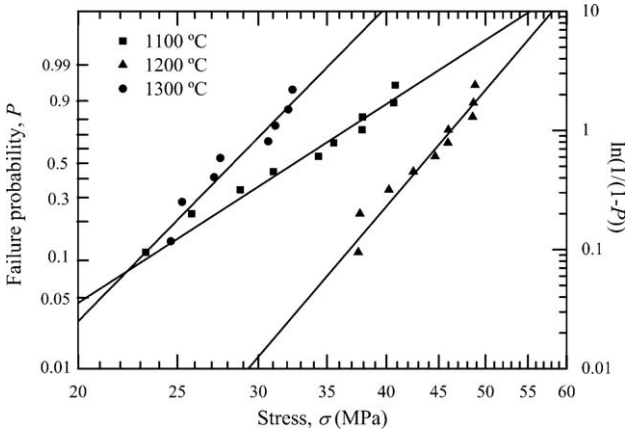

Fig. 9. Weibull 4-point bending strength plot (*i.e.*, failure probability *vs* applied stress) for β-TCP samples sintered for 3 h at the indicated temperatures. The straight lines are linear fits of the Weibull probability function (Eq. (1)) to data.

the sintering temperature from 1100 to 1200 °C significantly improves the strength (σ_f increases from 36.5 ± 0.4 to 46.3 ± 0.4 MPa) and reliability (m increases from 5.5 ± 0.6 to 10 ± 1) of β-TCP, as expected from the improvement in the material's density. On the contrary, increasing the temperature further up to 1300 °C reduces the strength of β-TCP ($\sigma_f = 30.5 \pm 0.3$ MPa, with $m = 8 \pm 1$) below the values measured at 1100 °C. Given the significant improvement in densification achieved at 1300 °C, this reduction in strength can only be attributed to the presence of microcracks.

The facts that microcracks are not observed at 1200 °C for all sintering times, and that the elastic modulus is reduced only after more than 3 h of sintering at this temperature, suggest that the residual stresses generated during the reversible $\beta \leftrightarrow \alpha$ transformation at 1125 °C are not high enough to develop cracks until the grains – and thus the precursor flaws – have grown to a certain critical size. One might argue that microcrack onset could also be related to an increase in the density of the material at longer sintering times, as porosity helps to relax residual stresses in the material. However, according to the data shown in Fig. 6, the differences in density between the samples sintered at 1200 °C for 3 h (crack-free) and 5 h (microcracked) are less than 1% while grain size increases by nearly 20%. According to these results the optimal sintering treatment for the particular TCP powders used here would be 3 h at 1200 °C, because these conditions produced a fair level of densification without the grains growing enough to generate microcracks.

4. Concluding remarks and implications

The results of the present study have allowed us to clarify the effect of sintering conditions (temperature and time) on the microstructure and mechanical properties of β-TCP samples fabricated from Ca-deficient commercial powders. Contrary to what has generally been accepted, the optimal sintering condition to maximize the mechanical performance of these materials is not necessarily located below the $\beta \leftrightarrow \alpha$ transformation temperature (1125 °C). In particular, optimal performance was achieved here in samples sintered at 1200 °C for 3 h, since it is not until higher temperatures or sintering times that microcracking develops and mechanical properties such as strength are greatly degraded. The residual stresses developed during the reversible transformation are not necessarily catastrophic for the mechanical integrity of the material. Sufficiently large starting flaws are necessary to trigger the development of the deleterious microcracks that are frequently reported for this material when it has been sintered above the transformation temperature. Unfortunately, TCP grain size increases rapidly at these sintering temperatures and microcracks develop before full densification can be achieved.

Based on this analysis, it emerges that a key guideline for processing dense β-TCP bioceramics with a good mechanical performance is grain refinement. Grain refinement can be achieved by reducing the particle sizes of the starting powders, and by using direct rapid heating techniques and/or grain-boundary segregants to minimize grain growth. Microstructure refinement will not only reduce the susceptibility of this material to transformation-induced microcracking, but will also improve the densification kinetics allowing TCP to be sintered at shorter times and/or lower temperatures.

These design guidelines constitute an opportunity to create β-TCP bioceramics with enhanced mechanical performance that may extend their range of application in orthopædics, which currently remains an open challenge.

Acknowledgements

This work was supported by the Ministerio de Educación y Ciencia (Spanish Government) and the Fondo Social Europeo under grant MAT2006-08720.

References

[1] N. Kondo, A. Ogose, K. Tokunaga, H. Umezu, K. Arai, N. Kudo, M. Hoshino, H. Inoue, H. Irie, K. Kuroda, H. Mera, N. Endo, Osteoinduction with highly purified [beta]-tricalcium phosphate in dog dorsal muscles and the proliferation of osteoclasts before heterotopic bone formation, Biomaterials 27 (25) (2006) 4419–4427.

[2] N. Kondo, A. Ogose, K. Tokunaga, T. Ito, K. Arai, N. Kudo, H. Inoue, H. Irie, N. Endo, Bone formation and resorption of highly purified [beta]-tricalcium phosphate in the rat femoral condyle, Biomaterials 26 (28) (2005) 5600–5608.

[3] A. Ogose, N. Kondo, H. Umezu, T. Hotta, H. Kawashima, K. Tokunaga, T. Ito, N. Kudo, M. Hoshino, W. Gu, N. Endo, Histological assessment in grafts of highly purified beta-tricalcium phosphate (OSferion) in human bones, Biomaterials 27 (8) (2006) 1542–1549.

[4] I.S. Cho, H.S. Ryu, J.R. Kim, D.W. Kim, K.S. Hong, Sintering behavior and microwave dielectric properties of tricalcium phosphate polymorphs, Japanese Journal of Applied Physics Part 1: Regular Papers Brief Communications & Review Papers 46 (2007) 2999–3003.

[5] H.H. Horch, R. Sader, C. Pautke, A. Neff, H. Deppe, A. Kolk, Synthetic, pure-phase betatricalcium phosphate granules (Cerasorb (R)) regeneration in the ceramic for bone reconstructive surgery of the jaws, International Journal of Oral and Maxillofacial Surgery 35 (8) (2006) 708–713.

[6] U.W. Jung, H.I. Moon, C. Kim, Y.K. Lee, C.K. Kim, S.H. Choi, Evaluation of different grafting materials in three-wall intra-bony defects around dental implants in beagle dogs, Current Applied Physics 5 (5) (2005) 507–511.

[7] M. Yoneda, H. Terai, Y. Imai, T. Okada, K. Nozaki, H. Inoue, S. Miyamoto, K. Takaoka, Repair of an intercalated long bone defect with a synthetic biodegradable bone-inducing implant, Biomaterials 26 (25) (2005) 5145–5152.

[8] M. Sous, R. Bareille, F. Rouais, D. Clement, J. Amedee, B. Dupuy, C. Baquey, Cellular biocompatibility and resistance to compression of macroporous beta-tricalcium phosphate ceramics, Biomaterials 19 (23) (1998) 2147–2153.

[9] P. Miranda, E. Saiz, K. Gryn, A.P. Tomsia, Sintering and robocasting of beta-tricalcium phosphate scaffolds for orthopaedic applications, Acta Biomaterialia 2 (4) (2006) 457–466.

[10] P. Miranda, A. Pajares, E. Saiz, A.P. Tomsia, F. Guiberteau, Mechanical properties of calcium phosphate scaffolds fabricated by robocasting, Journal of Biomedical Materials Research Part A 85A (1) (2008) 218–227.

[11] H.S. Ryu, H.J. Youn, K.S. Hong, B.S. Chang, C.K. Lee, S.S. Chung, An improvement in sintering property of beta-tricalcium phosphate by addition of calcium pyrophosphate, Biomaterials 23 (3) (2002) 909–914.

[12] R. Famery, N. Richard, P. Boch, Preparation of alpha-tricalcium and beta-tricalcium phosphate ceramics, with and without magnesium addition, Ceramics International 20 (5) (1994) 327–336.

[13] K. Itatani, T. Nishioka, S. Seike, F.S. Howell, A. Kishioka, M. Kinoshita, Sinterability of beta-calcium orthophosphate powder prepared by spray-pyrolysis, Journal of the American Ceramic Society 77 (3) (1994) 801–805.

[14] K. Lin, J. Chang, J. Lu, W. Wu, Y. Zeng, Properties of [beta]-$Ca_3(PO_4)_2$ bioceramics prepared using nano-size powders, Ceramics International 33 (6) (2007) 979–985.

[15] W.C. Oliver, G.M. Pharr, An improved technique for determining hardness and elastic-modulus using load and displacement sensing indentation experiments, Journal of Materials Research 7 (6) (1992) 1564–1583.

[16] W. Weibull, A statistical distribution function of wide applicability, Journal of Applied Mechanics: Transactions of the Asme 18 (3) (1951) 293–297.

[17] E. Sanchez-Gonzalez, P. Miranda, A. Diaz-Parralejo, A. Pajares, F. Guiberteau, Effect of sol–gel thin coatings on the fracture strength of glass, Journal of Materials Research 19 (3) (2004) 896–901.

[18] E. Sanchez-Gonzalez, P. Miranda, A. Diaz-Parralejo, A. Pajares, F. Guiberteau, Influence of zirconia sol–gel coatings on the fracture strength of brittle materials, Journal of Materials Research 20 (6) (2005) 1544–1550.

[19] E.R. Kreidel, F.A. Hummel, Two oxides. CaO–P_2O_5, Phase Diagrams for Ceramist, vol. II, 1969, 85–85.